International Journal of Students' Research in Technology & Management
eISSN: 2321-2543, Vol 6, No 3, 2018, pp 18-27
https://doi.org/10.18510/ijsrtm.2018.633

PROCESSING, DIELECTRIC, IMPEDANCE SPECTROSCOPY OF ELECTRONIC MATERIAL: $(Pb_{0.92}Ga_{0.08})(Zr_{0.48}Ti_{0.52})_{0.98}O_3$

[1*]Sugato Hajra, [1]PK Rout, [2]Sushrisangita Sahoo, [2]RNP Choudhary

[1] Department of Electrical and Electronics and [2]Department of Physics, Siksha O Anusandhan (deemed to be university), Bhubaneswar-751030, Orissa, India

*Corresponding author email: sugatofl@outlook.com

Article History: Received on 25th August, Revised on 08th October, Published on 18th October 2018

Abstract

Purpose of Study: The present work shows studies of some physical properties of a gallium (Ga) modified lead zirconate titanate $(PbZrTi)O_3$ with molar ratio Zr/Ti::48/52 (i.e., near morphotropic phase boundary (MPB)) having $(Pb_{0.92}Ga_{0.08})(Zr_{0.48}Ti_{0.52})_{0.98}O_3$ (PGaZT-8) as a chemical composition.

Methodology: The material was fabricated employing high-temperature mixed oxide route.

Main Finding: X-ray diffraction spectra suggest a distorted perovskite structure having two phases (tetragonal and monoclinic phases) with the substitution of small amount (2 and 4 wt %) of Ga in $Pb(ZrTi)O_3$ (PZT). However, with higher concentration of Ga (6 and 8 wt %) in PZT, the multiphase perovskite structure is converted into an orthorhombic system with few impurity phase of Ti_3O_5. Analysis of field emission scanning electron micrograph (FESEM) of 8 wt% Ga modified PZT (PGaZT-8) shows the uniform distribution but different dimension and shape of grains depicting high-density ceramic sample. In the dielectric studies no dielectric anomaly exists in the experimental temperature range (25-500ºC) in PGaZT-8, which determines the substitution of 8 wt% Ga in PZT (in MPB region) is found responsible for the suppression or shift (towards higher temperature) of known ferroelectric phase transition of PZT. There is an enhancement of permittivity, loss factor and conductivity as Pb site of PZT is doped with Ga.

Applications of study: This study is useful for determination of the characteristics of the prepared material as a base for device fabrication.

Novelty of the Study: It is a systematic study of correlation of structural properties with the physical properties. It helps to understand the relaxation and conduction mechanism of PGaZT-8 using impedance and modulus spectroscopy.

Keywords: Electronic Material, XRD, Solid State Reaction, Conductivity, Modulus

INTRODUCTION

With the rapid development of ceramic technology, some dielectric ceramic materials with higher energy storage density, temperature, structural stability and lower energy loss, are in great demand for their application in electronic and energy storage devices. Out of many oxides of various structural families, a number of ceramic oxides of perovskite family have gained huge interest of researchers in recent years due to their certain significant properties those needed for both present and future technological applications such as, memory storage devices, micro-electro-mechanical system, ceramic/multilayered capacitors, laser host etc (Muralt P., 2000; Scott J.F. 1989). Among most of the lead-based oxides, $PbTiO_3$ and its solid solution are extensively used for industrial applications. $Pb(ZrTi)O_3$ (PZT) is basically a solid solution of ferroelectric $PbTiO_3$ (Curie temperature (T_c)=490ºC) and antiferroelectric $PbZrO_3$ (T_c=230ºC) which acts as an excellent ferroelectric material (in ceramic and/or thin film form). Out of the four basic unit cell structures, namely the bismuth layered, tungsten-bronze, pyrochlore and oxygen octahedral form (i.e., ABO_3), the pure and doped PZT falls under the ABO_3 category. In PZT, Pb^{2+} and Zr^{4+}/Ti^{4+} ions occupy the A- as well as B-site respectively to maintain proper electrical neutrality and structural steadiness of the perovskite. The physical properties and structural stability of PZT solid-state solution (ceramics, composite or thin film) are tailored by suitable substitution(s) at A/B sites and/or varying Zr/Ti ratios for required devices (Panigrahi S.C. 2013). With modification of intrinsic (individual average domains response) and extrinsic (defect, dipoles, phase boundaries, etc) conditions, crystal symmetry and conduction mechanisms can be tailored (to get high dielectric and low tangent loss) of PZT ceramics for piezo-, pyro- and other applications (Arlt G. 1987). It is now a well established fact that the physical properties of PZT are affected by deviation of any factor like charge neutrality, solubility and ionic radius. Among these factors, Zr/Ti ratios are the most important because it strongly affects the structural and physical properties of PZT. For example, the 95/5 and 53/47 (Zr/Ti) ratios of PZT provide two MPB; where at lower temperature the structural phase transition shows transformation from orthorhombic to rhombohedral while higher temperature the rhombohedral to tetragonal transformation takes place respectively (Chamola A. 2011). The existence of both the structural phases at MPB enhances the dielectric and electrical characteristics of the material. Based on the above considerations, serious attempts have been made to develop PZT based electronic system by tailoring the dielectric, electrical, ferroelectric and other properties for devices, including manufacturing of pyroelectric detector for IR detection (Sen S. 2014). Panigrahi et al have cited the structural, electrical properties of pure PZ_xT_y (x/y=48/52) and Gd doped PZT bulk ceramics (Panigrahi S. C. 2014). Buixaderas et al studied the phase evolution, molecular and dielectric parameters of undoped soft/hard PZT ($PbZr_{0.42}Ti_{0.58}O_3$) (Buixaderas E. 2010). From the well established phase diagram and recent reports on PZT, it is clearly shown that it is formed in multiple phases (i.e. tetragonal, orthorhombic, rhombohedral,

pseudo tetragonal/ rhombohedral monoclinic) depends on Zr/Ti ratios, dopants and working temperature (Solanki R S. 2013). As reported earlier, the tetragonal and rhombohedral phases coexist in PZT MPB ceramics in most of the diffraction experiments (Zhang N. 2014; Mabud S.A. 1980; Cullity B.D. 1978). Some literatures also show that the XRD spectrum of a complicated PZT electronic system is influenced by internal structure and small size of the domain which form a two-phase system. In our recent investigations, the two structural phases (tetragonal and monoclinic) coexistence has been reported for the addition of a small amount of Ga in PZT (i.e., PGaZT-2 for 2 wt% and PGaZT-4 for 4 wt%) solid solution (Sharma P. 2017; Hajra S. 2017). On further addition of Ga (6 wt%) in PZT (referred as PGaZT-6), its X-ray diffraction pattern also shows multiphase. However, detailed analysis of XRD pattern/data shows that the best fit and agreement with experimental and model data (for all the reflections) can be obtained only in the orthorhombic system (Sharma P. 2017). As there are some anomalies in the above observations and reports on lower concentration of Ga-based PZT (MPB), it is required to examine the PGaZT system with a little higher concentration of Ga. The detailed literature survey also shows that some dielectric and electrical characteristics, such as permittivity, tangent loss, conductivity and impedance of modified PZT with small doping of 2 wt% of Ga have been tailored because of the creation of disordering and vacancies on replacing Pb^{2+} by Ga^{3+} (Sharma P. 2017). Due to the occurrence of these defects and long range ordering, ferroelectric and other properties of Ga-modified MPB PZT need more attention. Like $(PbLa)(ZrTi)O_3$, (PLZT), the Ga^{3+} has been added at the Pb^{2+}site in the parent compound $Pb(ZrTi)O_3$ by following substitution mechanism (i.e., compensating the charge balancing). In order to compensate the loss of Pb loss during the high temperature calcination and sintering and charge compensation (due to high volatile nature of lead and reaction occurring in a PbO atmosphere), we added a small amount of PbO. However no experimental evidence has been shown that gallium ions have gone to B-sites, instead the A-sites only because B-site vacancies are favoured more under increased PbO vapour pressure (Hardtl K.H. 1972).The sharing of ion on the sites (A- or B-) seems to be a regular function of ionic radius. A larger ionic radius favours A- site (Jaffee B. 1971). The conductivity study largely influences many properties (piezoelectric, pyroelectric and other properties) of ferroelectric materials.

In this context, the conduction mechanism has not been clearly investigated with respect to the impedance and modulus spectroscopy. We have already investigated the effect of small amount of Ga (at the Pb-site) on the above physical properties of PZT (i.e., $Pb_{1-x}Ga_x(Zr_{0.48}Ti_{0.52})_{0.98}O_3$; x= 0.02, 0.04, 0.06). Some interesting results of these materials have already been compared with those of parent compound PZT (Sharma P. 2017; Hajra S. 2017). In this context, we have attempt to study the phase formation, micro-structural, dielectric and electrical (conductivity, impedance, modulus) properties of higher content (8 wt %) of Ga in PZT (i.e., $Pb_{0.92}Ga_{0.08}(Zr_{0.48}Ti_{0.52})_{0.98}O_3$ (PGaZT-8)) to provide useful data and suitable explanation of the conduction mechanism of the material.

EXPERIMENTAL PROCEDURES

A high-temperature mixed-oxide reaction method was employed to synthesize $Pb_{0.92}Ga_{0.08}(Zr_{0.48}Ti_{0.52})_{0.98}O_3$ (PGaZT-8) using high-purity or analytical grade oxides, like PbO, TiO_2 (99.5%, Loba Chemie), Ga_2O_3 (99.999%, OTTO-Chemika-Biochemica-Reagents) and ZrO_2 (99%, Himedia). Based on the particle size and purity of oxides, the raw materials are selected for achieving chemical equilibrium. The powder of raw materials is carefully weighed in a required stoichiometric proportion using digital balance to synthesize the sample. To prepare a uniform mixture of the raw ingredients, it is ground in dry atmosphere and further mixing methanol for all total 4 hrs by the help of pestle and agate mortar. The homogeneously mixed fine powder was then calcined for 4 hrs at 1000 ^oC. During high-temperature processing of the material, 2 wt% of PbO was additionally put into the mixture to overcome the expected lead loss and maintain desired stochiometry after processing. The calcinated powder was thoroughly mixed with polyvinyl alcohol (binder) to fabricate green pellets. The compact cylindrical pellets of a desired dimension (12 mm diameter and 1–2 mm of thickness) were prepared under 4 x 10^6 N/m^2 pressure. The pellets were initially fired at different temperatures starting from 900^oC (with increasing temperature interval of 25 ^oC) to optimise sintering temperature. The pellets were finally sintered at 1025^oC in air in a conventional furnace for 4 hrs. X-ray powder diffractometer (Bruker D8 Advance, Cu target) was used to collect diffraction data to be used to determine the basic crystal data, phase- purity and quality of the sample prepared (PGaZT-8). The X-ray data were recorded at room temperature with increment of 0.04^o using Cuk_α radiation (wavelength λ=1.5418 Å) and wide Braggs angle. The micrograph of the pellet sample was recorded using ZEISS EVO10 FESEM functioning at 20.0 kV. The FESEM image was captured from a gold-coated sample for better image showing the grain distribution and degree of porosity. A zero level of emery paper was taken to polish one of the sintered pellet and then silver electrode was painted upon both sides of the pellet for electrical characterization. The electroded sample was dried at 120^oC for 4 hrs before carrying out measurements of dielectric and electrical parameters. The electrical properties (dielectric, impedance, tangent loss) are measured over a frequency ranging from 1 kHz-1MHz at temperatures between 25-500°C using PSM 4NL phase sensitive meter. A thermocouple of K type and digital panel (Rishabh N25) meter were used to observe the rise in sample holder temperature.

RESULTS AND ANALYSIS

3.1 Phase Formation:

Figure 1 presents the X-ray diffraction spectra of PGaZT-8 at room temperature. The experimental XRD spectra were matched with a reported pattern (JCPDS No. 01-070-4261) using a software package *"X'pert highscore* plus (version

3.0.5)" (Joseph J. 2000). Analysis of XRD pattern also shows that marked (as *) peaks belong to Ti_3O_5 (JCPDS No. 01-072-0519) (Asbrink S. 1957). The best fit matched data suggest an orthorhombic symmetry by calculating the minimum difference value in the observed (obs) and calculated (cal) interplanar spacing (d). The least-squares refinement subroutine of POWDMULT (version 2.2) software package was used to calculate lattice parameters indexing all the peaks. It is observed that a few small intensity impurity peaks are also available. After the indexing of the peaks, it was found that the PZT structure has been modified from reported normal tetragonal to distorted perovskite in orthorhombic structure on addition of Ga (8 wt %). The least-squares refined lattice parameters of major phase of PGaZT-8 in the orthorhombic crystal system are: a=4.1256 Å, b=8.7543 Å and c=29.9471 Å which is to be normalized to a new unit cell; a´= 2a=8.2512Å, b´=b=8.7543 Å and c´=c/2√3=8.6431Å. This normalized orthorhombic cell is equivalent and consistent with those of distorted perovskite reported earlier for PGaZT-6 (Sharma P. 2017).

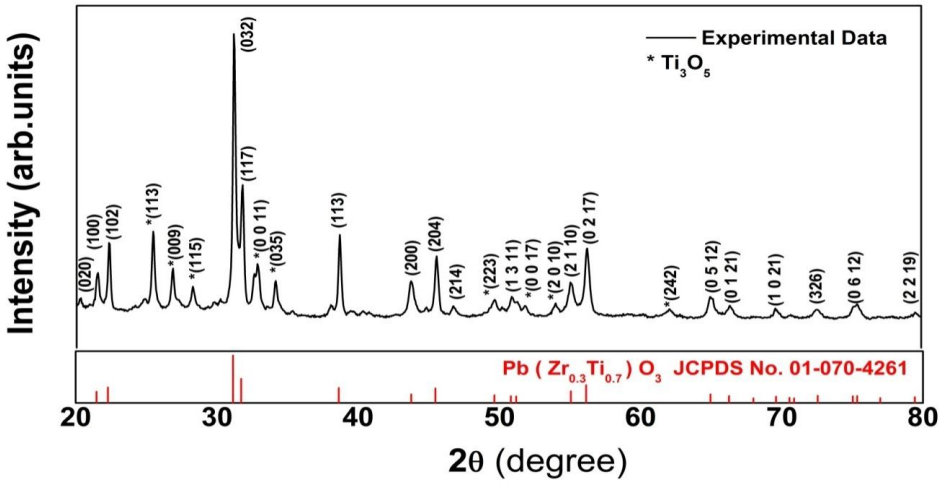

Figure 1: Room temperature XRD spectra of PGaZT-8 sample

3.2 Microstructure analysis

The surface micrograph of reported PZT represents the uniform distribution of varying size of grains. The average estimated grain size is obtained to be 1-2 µm. In 2 wt % of Ga modified PZT, there was growth of non-uniform grains of different shape and size. In case of 4 and 6 wt % addition of the Ga in PZT system, the surface morphology depicts non uniform distribution of spherical and rectangle grains with high density growth (Sharma P. 2017). Figure 2 manifests the morphology; the topography and texture of the sintered pellet studied under a higher resolution field emission scanning electron microscope (FESEM). To lessen the charging effect and enhanced conductive surface during the investigation a gold film was sputtered. An uneven distribution with two different shapes (rectangular and small spherical) is obtained. A dense (minimum porosity degree) and a crack free morphology is seen with x=0.08 of Ga-substitution in PZT. Due to lack of experimental software we could not calculate the degree of porosity. The texture and distribution of grains of the sample confirm polycrystalline nature of the material. As the kinetics of fabricated bulk sample is complex, it is quite difficult to examine the changes in grain shape, size and texture.

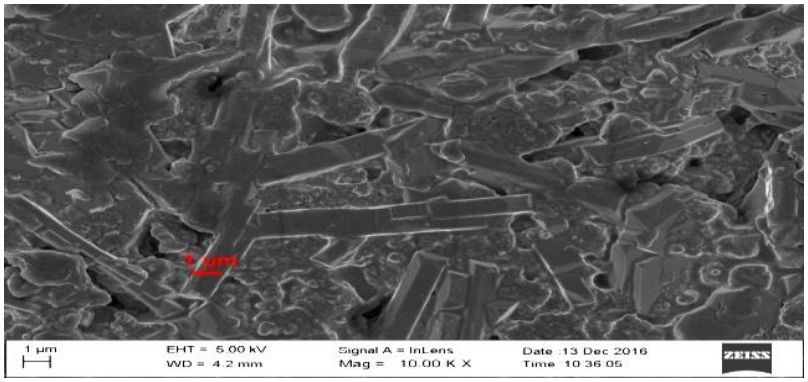

Figure 2: FESEM micrograph of PGaZT-8 sintered sample

3.3 Dielectric Study

The magnitude of dielectric constant of PZT (based on temperature dependent plots of dielectric constant) was reported to be 2978 at 10 kHz which reduces to 2162 at 1000 kHz. The transition temperature (T_c) was observed at 432ºC at all the studied frequencies (Panigrahi S. C. 2014). In the dielectric constant vs. temperature plots (at different frequency) of the

International Journal of Students' Research in Technology & Management
eISSN: 2321-2543, Vol 6, No 3, 2018, pp 18-27
https://doi.org/10.18510/ijsrtm.2018.633

PGaZT-2, PGaZT-4, and PGaZT-6 samples, we observe that the T_c shifts to the higher temperature side on addition of Ga in PZT (Sharma P. 2017). Figure 3 (a) exhibits the variation of dielectric permittivity with temperature for PGaZT-8 at various frequencies in the range of 10^3 Hz-10^6 Hz. It clearly shows that dielectric constant increases steadily with the rise in temperature without showing any dielectric anomaly in the experimental temperature region. We did not observed any dielectric anomaly in PGaZt-8 (in the low frequency region) to show the existence of reported ferroelectric–paraelectric phase transition of PZT which may be due to the shift of transition temperature beyond our experimental temperature limit or suppression of phase transition due to symmetry change from polar to non-polar structure. However, at higher frequency (>500 kHz), a phase transition (T_c) was observed around 450°C which may be beneficial in development of high temperature piezoelectric devices. In case of low content (<6%) Ga modified PZT (i.e., PGaZT-2, -4, -6), the magnitude of dielectric permittivity increases with temperature rise at all the frequencies (Sharma P 2017; Hajra S. 2017) Figure 3 (b) presents the decreasing trend of dielectric permittivity with increasing frequency for doped samples at some temperatures. The contributions of some polarizations (i.e., interfacial, ionic, dipolar, electronic) may be considered a main reason for the higher value of permittivity at lower frequencies (Frantti J. 2000). The dielectric constant decreases at higher frequencies as some of the polarizations (except electronic) become futile. At the lower frequency the magnitude of dielectric permittivity rises due to interfacial polarization, but at higher frequencies it becomes ineffective.

Figure 3 (c) displays a normal behavior of ferroelectric materials which is strongly indicated by the decreasing trend of loss factor (tan δ) with rise in frequency. In this case, lag of polarization follows the applied electric field which is mainly due to impurities and imperfection (Sahu M. 2017). This plot shows high energy loss (tan δ) at low frequencies which arises due to higher conductivity attributed by ionic space-charge carriers like Ga (Sun L. 2015). Other that ionic nature of Ga, the sintered ceramic sample has defects and the oxygen vacancies. Apart from this, Figure 3 (d) shows the small value of tan δ up to 400 ° C, and then it shows a significantly increasing trend. The contribution of space charge polarization can also be added to the value of tan δ to observe higher value of the loss factor.

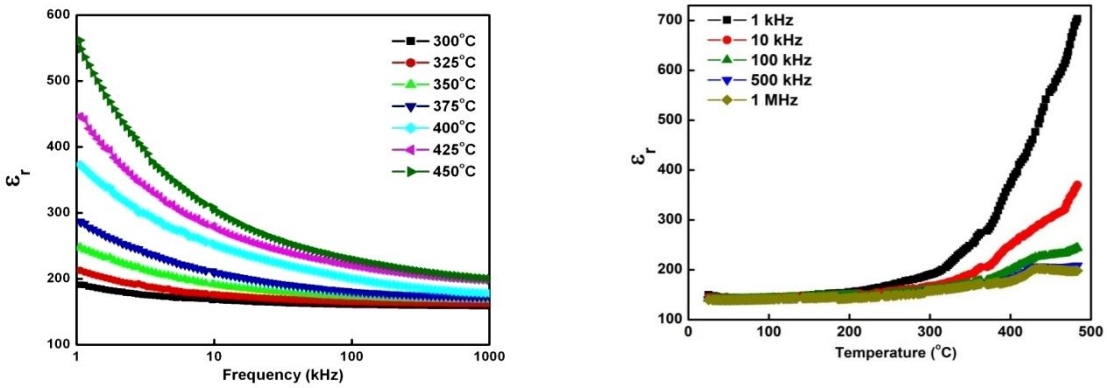

Figure 3(a) Temperature dependent dielectric permittivity and (b) Frequency dependent dielectric permittivity of PGaZT-8

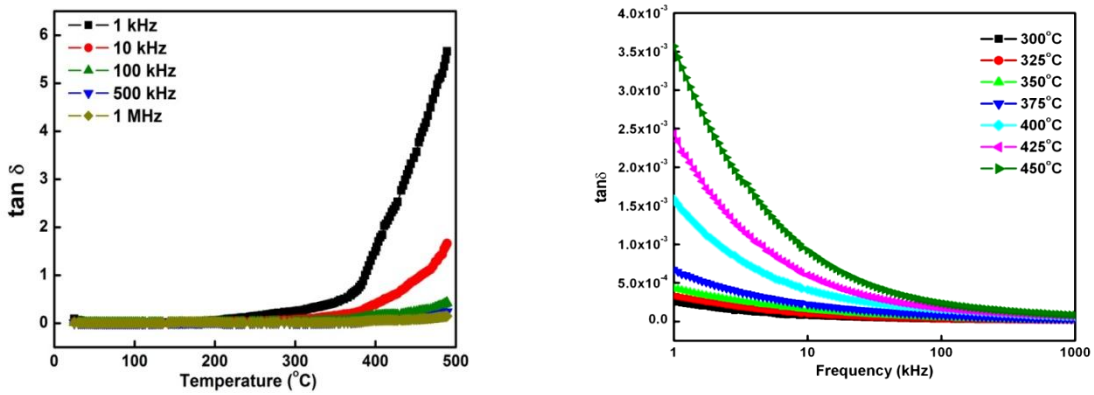

Figure 3 (c) Temperature dependent dielectric loss and (d) Frequency dependent dielectric loss of PGaZT-8

3.4 Conductivity

The association of diverse physical properties with the response to the electrical signal can be investigated by means of electrical conductivity. In the perovskite structure (ABO_3) the presence of defects/oxygen vacancy are held responsible for

polarization in crystal. Figure 4(a) presents the inverse of absolute temperature with AC conductivity at selected frequencies. The relation $\sigma_{a.c.} = \omega\varepsilon_0\varepsilon_r \tan\delta$ where all symbols have their usual meaning is helpful for obtaining the AC conductivity of the prepared sample. It is observed that with increase in frequency, there is a rise in AC conductivity. The temperature vs. AC conductivity curves can be obtained by a frequency independent Arrhenius equation; $\sigma = \sigma_0 exp(\frac{-E_a}{k_B T})$ or $\ln\sigma = -E_a / k_B T + \ln\sigma_o$ where σ_0 is constant, k_B is the Boltzmann constant, and E_a is the activation energy (Maity S. 2011). The linear fitting of ln σ_{ac} vs 1000/T for various temperature regions helps to calculate the activation energy. The temperature dependent conductivity used to calculate the activation energy and changing its value from 0·66 to 1.11 eV (depending on frequency). The conduction process is a thermally activated mechanism of the charge carriers. In perovskite ferroelectrics, the motion of oxygen vacancies (primary mobile charge carriers) gives a boost to activation energy (Sahu N. 2013). During sintering, the oxygen vacancies occur due to loss of oxygen, and the charge composition follows the universal Kroger-Vink equation (Chandran A. 2011):$O_o \rightarrow O_o\uparrow + V_o^{\cdot\cdot} + 2e^{-1}$.

In PGaZT-4, activation energy (from 1 kHz to 100 kHz) is ranging from 0.793 eV- 0.659 eV. In this case, the activation energy of PGaZT-6 has been calculated with two slopes of the curves (from 1 kHz- 500 kHz) and found in the range of 1.26- 0.63 eV and 0.52- 0.32 eV. At 100 kHz, the value of activation energy of PZT, PGaZT-4, PGaZT-6 has been reported to be 0.57, 0.66, 0.49 eV respectively (Hajra S 2017; Sharma P 2017; Panigrahi S.C. 2014). The frequency dependent AC conductivity in Pure PZT, PGaZT-4, PGaZT-6 has been reported from $1x10^{-3}$ to 0.01 $\Omega^{-1}m^{-1}$, 0.0002 to 0.002 $\Omega^{-1}m^{-1}$, 0.0003 to 0.0019 $\Omega^{-1}m^{-1}$ respectively (Hajra S 2017; Sharma P 2017; Panigrahi S.C. 2014).

Figure 4 (b) provides the frequency response of AC conductivity. The curves are fitted to the Jonscher's equation; $\sigma_{ac}=A\omega^n$. The first term of the equation explains the frequency independent contribution (flat region at low frequency is equivalent to DC conductivity) and the second term explains the frequency variant contribution (dispersive region) to the total conductivity. The table 1 shows the fitting parameter values of A and n. As reported earlier, there are different conduction mechanisms such as small Polaron hopping, correlated barrier hopping, quantum mechanical tunnelling and overlapping large Polaron tunnelling which represent the temperature dependence of frequency exponent n. Table 1 shows the change (decrease and increase) of frequency exponent. It initially decreases up to 350°C, and then increases with temperature rise. This feature can be explained by overlapping large Polaron tunnelling model and suggests the conduction mechanism (Barick B.K. 2012)

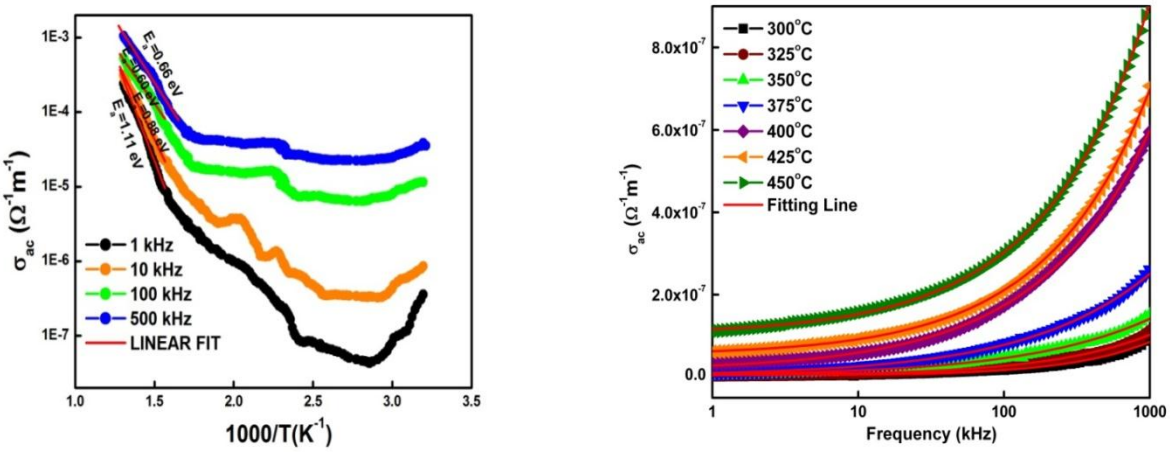

Figure 4 (a) Variation of (a) AC conductivity vs inverse temperature at frequency and (b) AC conductivity with frequency at different temperatures for PGaZT-8.

3.5 Impedance Study

The sharing of (i) grains, (ii) grain boundary and (iii) electrode effect in the resistive and capacitive characteristics of solids, particularly ceramics and ionic conductors, can be studied using the complex impedance spectroscopy (CIS). Besides this, the characterization of the electrical behavior/ dynamics of mobile ions in ionic conductors, ferroelectrics and other ceramic compounds over a wide range of temperature and frequency by this CIS technique. The CIS data may be plotted by several ways using complex impedance formalism (Acharya T. 2015). Among all the formalism, the complex impendence plot, Nyquist plot (Z″ on the y-axis vs Z′ on the x-axis) is important for finding the relaxation processes and conduction mechanism present in the prepared sample. The frequency dependent electrical properties are usually exhibited in terms of complex admittance (Y*), permittivity (ε*), modulus (M*), loss tangent (tan δ) and complex impedance (Z*) which are also associated with each other. The temperature and frequency dependent Z* (real and imaginary parts) are calculated using some basic equations (Chaisan W. 2005):

(1) Dielectric loss: $\tan\delta = \frac{\varepsilon''}{\varepsilon'} = -\frac{z'}{z''} = \frac{M''}{M'}$

(2) Complex Modulus: $\frac{1}{\varepsilon^*} = M^* = M' + jM'' = j\omega C_o Z^* * \omega$

(3) Complex impedance: $z^* = z' - z'' = R_s - \frac{j}{\omega C_s}$

(4) Complex permittivity: $\varepsilon^* = \varepsilon' - j\varepsilon''$

(5) Complex admittance: $Y^* = Y' + Y'' = \frac{1}{R_p} + j\omega C_p$

$M' = -\omega C_0 Z$ and $M'' = \omega C_0 Z'$ ----- (6)

The real and imaginary part of the impedance is described by the following equation:

$$Z' = \frac{R}{1+(\omega\tau)^2} \text{ and } Z'' = \frac{\omega R\tau}{1+(\omega\tau)^2} \quad \text{------ (7)}$$

Where the symbols have their usual meaning.

Figure 5 (a) shows that Z' decreases at the low-frequency region with rise in temperature where as it declines and attains a constant value at the region of higher frequency. This nature of variation of Z′ (i.e., negative temperature coefficient of resistance) suggests the semiconductor behaviour of the sample. Based on the impedance plots, it has been reported that PZT, PGaZT-2, PGaZT-4, PGaZT-6 have non-Debye type of dielectric relaxation. The frequency dependent real part of the impedance plot at 300ºC (at 1 kHz) is found to be 110, 175, 240, 1400 kΩ for PZT, PGaZT-2, PGaZT-4, PGaZT-6 respectively (Hajra S 2017; Sharma P 2017; Panigrahi S.C. 2014).
Figure 5 (b) shows the frequency-temperature dependence of Z″ which suggests the resistive nature of the sample. The two relaxation mechanisms of different relaxation time are obtained by careful analysis of spectrum. The grain effect explains higher frequency peak region (Behera C. 2014)
Other than the above role of complex impedance plot, it helps to analyse AC conductivity. The dominant resistance of the sample can be determined by these plots. In case of smaller resistance, the plot is not very conclusive and sensitive to determine conduction mechanism. But, the nature of the semiconducting arcs helps to distinguish the type of relaxation mechanisms (Debye or Non-Debye) present in the system. Each perfect semicircular arc (center falling at Z'axis) is a signature of the Debye relaxation mechanism which explains the grain homogeneity and existence of mono relaxation time in the material (Pattanayak S. 2014). Similarly, the depressed semicircles of Z'vs. Z'' plot is a signature of Non-Debye type of relaxation process indicating the inhomogenity in grain size and electromagnetic diffusion (Garbarz-Glos B 2013; Mishra R K. 2014).
The high-frequency semicircle explains the bulk properties of the material whereas the grain size effect is attributed to the low-frequency semicircles. The computer-controlled software package (ZSIMP WIN version 2.0) is used to fit the theoretically calculated data with experimental data for knowing the type of the relaxation mechanism (Debye or non-Debye type). The fitted plot and the equivalent electrical circuit (a circuit comprising of resistors that represents the conductive path and capacitors representing the space charge polarization is proposed; RQC model, Q=constant phase element) analogous to the sample impedance response is shown as an inset in Figure 5 (c). The conduction process is due to the effect of grains, which is clearly seen from the fitted plot and the electrical model used. The depressed or distorted semicircle of the plot clearly identifies the Non-Debye relaxation process. The deviation from an ideal Debye behavior has been modified by adding the constant phase element in the modelled circuit (Xia J. 2014).
The values of grain capacitance, grain resistance and apparent bulk conductivity of the sample by using the fitted curves at various temperatures are given in Table 2. Using the values of grain resistance (R_g), DC conductivity is calculated by the formula = t/ R_gA, where t shows the thickness of the sample and A shows deposition area of the electrode. The relative permittivity of the prepared material can be calculated using impedance spectroscopy data. The fitted capacitance value (Cg), free space dielectric constant value (ε_o) =8.85x10^{-12} and geometric dimensions (thickness (d), area (a)) of sample help to estimate the relative permittivity by a formula (ε=Cd/ε_oA). It is seen with rise in temperature, the resistance of the sample increases on increasing temperature from 300 to 350ºC which shows semiconductor behaviour with positive temperature coefficient of resistance. Further, an increase in temperature decreases the grain resistance, which is an efficient analogous to the negative temperature coefficient of resistance (NTCR) indicating semiconducting behaviour of the doped sample (Purohit V. 2018). Figure 5(d) is drawn to show the Nyquist plot at (475 and 500) ºC with equivalent

International Journal of Students' Research in Technology & Management
eISSN: 2321-2543, Vol 6, No 3, 2018, pp 18-27
https://doi.org/10.18510/ijsrtm.2018.633

circuit model. The non-Debye type behavior is also confirmed from Figure 5(d) inset depicts a depression angle of 21.44° and it is observed that the center lies below the real Z axis at 500 °C.

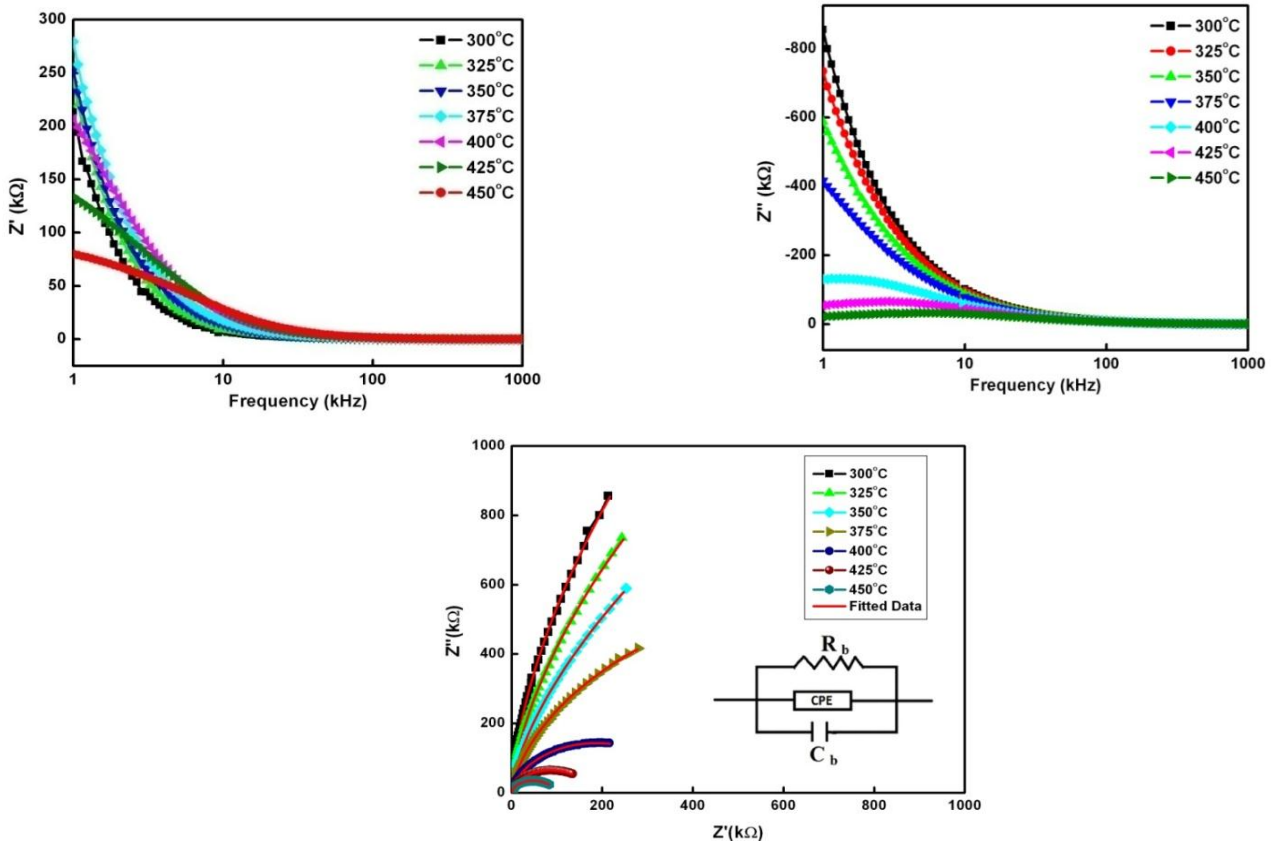

Figure 5 (a) Frequency dependent Z' at different temperatures, (b) variation of Z" with frequency at different temperatures (c) variation of Z" with Z' for sample PGaZT-8 at selected temperatures

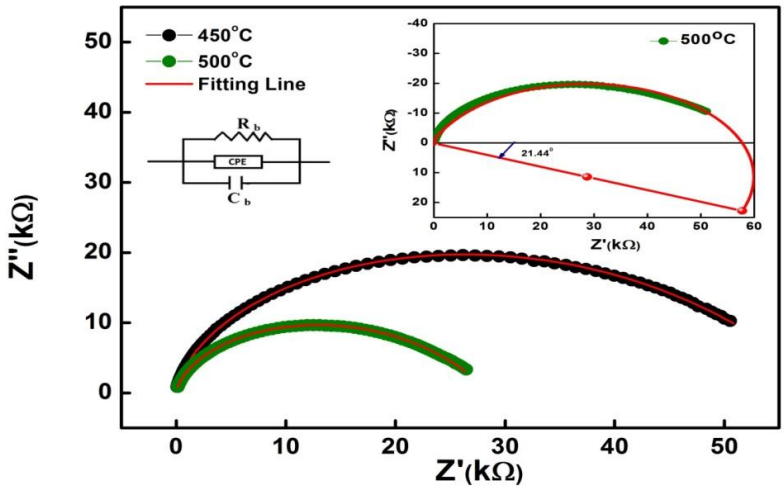

Figure 5(d) Nyquist Plot for temperature 450°C, 500°C and (inset) shows the equivalent circuit model along with depression angle at 500°C

3.6 Complex Electric Modulus Study

The electrical modulus analysis helps to determine the (1) grain boundary conduction effect, (2) electrical conductivity (3) electrode polarization (4) relaxation time and (5) bulk properties in the fabricated specimen at different temperatures and frequencies.

In case of PGaZT-2, PGaZT-4, PGaZT-8, the frequency dependent variation of real and imaginary part of modulus is as follows: In case of the real part of modulus, all of them manifests increase in the magnitude of M´ at lower frequency. At higher frequency, there is dispersion. But in case of frequency dependent imaginary part of modulus, the peak shifts

towards the high frequency side depicting a thermally assisted process in all the mentioned samples (Hajra S 2017; Sharma P 2017; Panigrahi S.C. 2014).

With an increase in frequency, a continuous dispersion in the Ga doped PZT sample is obtained in the M′ vs. frequency plot. Based on the conduction phenomena, above characteristics suggest the presence of short range mobility of charge carriers in the material. Generally, the mobility of charge carriers depends on the restoring force induced by the applied field. The short range mobility of charge carrier suggests the restoring force deficiency which governs the charge carriers during the conduction process (Kumar A. 2007)

Figure 6 (b) exhibits that on increasing temperature, the peak position of M''_{max} shifts to the higher frequency side. There are three regions in the imaginary part of the modulus: region I represent the below peak frequency mechanisms, region II represents the peak frequency (transition) and the region III represents the after peak frequency mechanisms. Region I corresponds to the range in which the charge carriers are mobile over long distances. Region II satisfies the condition; $\omega_m\tau_m = 1$, where ω_m is the angular frequency corresponding to M″ maximum and τ_m is the relaxation time. Region III indicates the charge carriers are trapped in a potential well, so they are mobile over short distances. Region II indicates the transition from a region I (long range mobility) to region III (short range mobility). At the high temperature, the peaks gradually shifted which suggested in a thermally activated relaxation process. The asymmetric and broader peaks in the plots are the indicator of Non-Debye type relaxation (as explained earlier in the impendence study) Sutar B. C. 2014, MacDonald J. R. 1984)

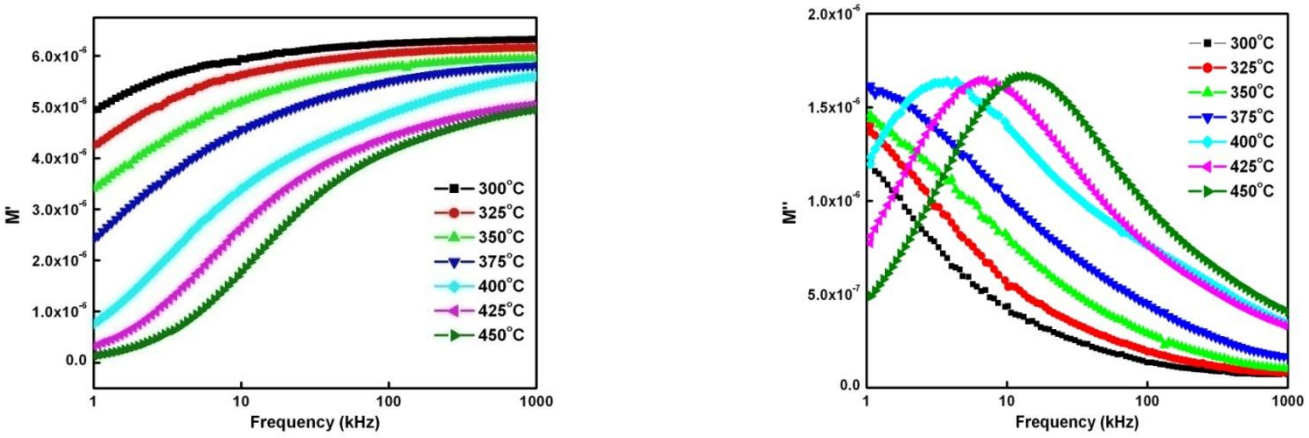

Figure 6: Variation of (a) M' with frequency at different temperatures (b) M" with frequency at different temperatures of PGaZT-8

CONCLUSION

Polycrystalline sample of PGaZT-8 has been prepared by a cost effective mixed oxide (solid state reaction) method. On the substitution of small amount of Ga (<6%), the unit cell of the sample has been distorted from tetragonal (structure of parent sample) to tetragonal (major) and monoclinic (minor) phases showing existence of two phases system (disrupted perovskite system). However, the PGAZT-8 is finally converged in distorted perovskite orthorhombic phase with few secondary phases. There is a non-uniform grain distribution on the pellet surfaces. Thus, a low-loss material is depicted from high-density grains and low-dielectric loss as reported above. The Ga-substitution at the Pb-site of PZT either shifts the reported transition temperature (of PZT) beyond experimental temperature or suppresses the ferroelectric characteristics. The frequency dependent the imaginary part of impendence and modulus suggests the occurrence of non-Debye relaxation process. The nature and magnitude of modulus peaks observed in the plots suggest the movement from long to short range mobility of charge carriers which is closely associated to the conduction phenomena. The frequency and temperature response of conductivity follow the power law of Jonscher. The material (PGaZT-8) may be used as a component of electronic devices as per the above results obtained.

CONFLICT OF INTEREST AND ETHICAL STANDRADS

The authors have no conflict of interest. Sugato Hajra, Sushrisangita Sahoo fabricated the material and performed the electrical characterization. Sugato Hajra and Dr. PK Rout contributed in writing the article. Dr. RNP Choudhary supervised the work. All the authors contributed towards the discussion of the analysis.

ACKNOWLEDGEMENT

SH like to thanks Mr. Uttam Chandra and Mr. Manas Sahoo, IIT Bhubaneswar for their help in doing some experiments (XRD, SEM).

REFERENCES

[1] Muralt P., (2000) PZT thin films for microsensors and actuators: Where do we stand? *IEEE Trans. Ultrason., Ferroelect., Freq. Control* 47, 903–915, https://doi.org/10.1109/58.852073
[2] Muralt P., (2000) Ferroelectric thin films for micro-sensors and actuators: a review. *Journal of micromechanics and micro engineering* 10, 136, https://doi.org/10.1088/0960-1317/10/2/307
[3] Scott J.F., Dearaujo C.A.P., (1989) Ferroelectric Memories. *Science* 246, 1400-1405, https://doi.org/10.1126/science.246.4936.1400
[4] Panigrahi S.C., Das P R, Parida B.N, Sharma H B K, Choudhary R N P, (2013) Effect of Gd-substitution on dielectric and transport properties of lead zincronate titanate ceramics. *J mater Sci: Mater Electron* 24, 3275-3283, https://doi.org/10.1007/s10854-013-1243-x
[5] Arlt G., Dederichs H., Herbiet R., (1987) 90°-domain wall re-laxation in tetragonally distorted ferroelectric ceramics. *Ferroelectrics* 74, 37-53, https://doi.org/10.1080/00150198708014493
[6] Chamola A., Singh H, Naithani U.C., Sharma S et al. (2011) Structural, dielectric and electrical properties of Lead zirconate titanate and CaCu3Ti4O12 ceramic composite. *Adv. Mat. Letters* 2, 26-31, https://doi.org/10.5185/amlett.2010.12182
[7] Sen S., Choudhary R.N.P, Pramanik P., (2007) Structural and electrical properties of Ca2+-modified PZT electroceramics. *Physica B* 387, 56-62, https://doi.org/10.1016/j.physb.2006.03.028
[8] Panigrahi S. C., Das P R., Parida B. N., Padhee R., Choudhary R. N .P., (2014) Dielectric and electrical properties of gadolinium-modified lead-zirconate-titanate system. *Journal of Alloys and Compounds* 604, 73–82 , https://doi.org/10.1016/j.jallcom.2014.03.078
[9] Buixaderas E., Nuzhnyy D., Vaněk P., Gregora I., Petzelt J. et al. (2010) Lattice dynamics and dielectric response of undoped, soft and hard PbZr0.42Ti0.58O3, *Phase Transit*. 83, 917 , https://doi.org/10.1080/01411594.2010.509601
[10] Solanki R S., Mishra S K, Senyshyn A, Yoon S, Baik S, Shin N, Pandey D. (2013) Confirmation of the monoclinic Cc space group for the ground state phase of Pb(Zr0.525Ti0.475)O3: A combined synchrotron X-ray and neutron powder diffraction study . *Applied Physics Letter* 102, 052903, https://doi.org/10.1063/1.4790569
[11] Zhang N, Yokota H, Glazer AM, Ren Z, Keen DA, Keeble DS, Thomas PA, Ye ZG. (2014) The missing boundary in the phase diagram of PbZr(1-x)TixO_3 *Nature communications* 5, 5231
[12] Mabud S.A. (1980) The morphotropic phase boundary in PZT solid solutions. J Appl Crystallogr 13, 211-216 , https://doi.org/10.1107/S0021889880011958
[13] Cullity B.D., (1978) *"Elements of x-ray diffraction",* Addison-Wesley Pub: Reading, Mass ,
[14] Sharma P, Hajra S, Sahoo S, Rout P K, Choudhary R N P (2017) Structural and electrical characteristics of gallium modified PZT ceramics. *Processing and Application of Ceramics* 11, 171-176 , https://doi.org/10.2298/PAC1703171S
[15] Hajra S, Sharma P, Sahoo S, Rout P K, Choudhary R N P. (2017) Processing and electrical properties of gallium-substituted lead zirconate titanate ceramics . *Applied Physics A*, 123:786, https://doi.org/10.1007/s00339-017-1411-6
[16] Sharma P, Hajra S, Sahoo S, Rout P K, Choudhary R N P., (2017) Capacitive and resistive characteristics of gallium modified lead zirconate titanate. *J material SCI: Mater electron* 28, 12048-12055, https://doi.org/10.1007/s10854-017-7016-1
[17] Hardtl K.H., Hennings D., Distribution of A-Site and B-Site Vacancies in (Pb, La)(Ti, Zr)03 Ceramics. (1972) *J. Am. Ceram. Soc*. 55, 230-231, https://doi.org/10.1111/j.1151-2916.1972.tb11267.x
[18] Jaffee B., WR Cook Jr. , Jaffe H. (1971) *Piezoelectric ceramics,* Academic Press, New York
[19] Joseph J., Vimala T.M., Sivasubramanian V, Murthy V R K (2000) Structural investigations on Pb(ZrxT1−x)O3 solid solutions using the X-ray Rietveld method. *Journal of Materials Science* 35, 1571-1575 , https://doi.org/10.1023/A:1004778223721
[20] Asbrink S., Magneli A., (1957) Note on the Crystal Structure of Trititanium Pentoxide. *Acta Chem. Scand.*, 11, 1606, https://doi.org/10.3891/acta.chem.scand.11-1606
[21] Frantti J., Lappalainen J., Lantto V., Rundlof H., Nishio S., Eriksson S., Ivanov S., Kakihana M. (2000) Neutron diffraction studies of Pb(ZrxTi1-x)O-3 ceramics. *Jpn. J. Appl. Phys.* 39, 5697-5703 , https://doi.org/10.1143/JJAP.39.5697
[22] Sahu M., Choudhary R.N.P., Das S., Otta S., Roul, B.K. (2017) Inter-grain mediated intrinsic and extrinsic barrier layer network mechanism involved in Ca1Cu3Ti4O12 bulk ceramic. *J. Mat. Science: Materials in Electronics* 28 15676–15684 , https://doi.org/10.1007/s10854-017-7457-6
[23] Sun L., Wang Z., Shi Y., Cao E. et al (2015) Sol–gel synthesized pure CaCu3Ti4O12 with very low dielectric loss and high dielectric constant. *Ceram. Int.* 41, 13486-13492 , https://doi.org/10.1016/j.ceramint.2015.07.140
[24] Maity S., Bhattacharya D, Ray S K (2011) Structural and impedance spectroscopy of pseudo-co-ablated (SrBi2Ta2O9)(1−x)–(La0.67Sr0.33MnO3)x composites. *J. Phys. D: Appl. Phys.* 44, 095403 , https://doi.org/10.1088/0022-3727/44/9/095403
[25] Sahu N., Panigrahi S. (2013) Rietveld analysis, dielectric and impedance behaviour of Mn3+/Fe3+ ion modified Pb (Zr0•65Ti0•35)O3 perovskite. *Bull. Mater. Sci.* 36, 699–708 , https://doi.org/10.1007/s12034-013-0522-8
[26] Chandran A., Samuel M. S, Koshy J., George K.C. (2011) Dielectric relaxation behavior of CdS nanoparticles and nanowires *J. Mater. Sci.* 46, 4646–4653 , https://doi.org/10.1007/s10853-011-5368-0

[27] Barick B.K., Choudhary R.N.P., Pradhan D K. (2012) Phase transition and electrical properties of lanthanum-modified sodium bismuth titanate. *Materials Chemistry and Physics* 132, 1007– 1014 , https://doi.org/10.1016/j.matchemphys.2011.12.050
[28] Acharya T., Choudhary R N P. (2015) Development of Ilmenite-type Electronic Material CdTiO3 for Devices. *IEEE Transactions on Dielectrics and Electrical Insulation* 22, 3521 , https://doi.org/10.1109/TDEI.2015.005196
[29] Chaisan W., Yimnirun R., Ananta S., Cann. D.P. (2005) Dielectric properties of solid solutions in the lead zirconate titanate–barium titanate system prepared by a modified mixed-oxide method. *Mater. Lett.* 59, 3732-3737, https://doi.org/10.1016/j.matlet.2005.06.045
[30] Behera C., Das P R., Choudhary R.N.P. (2014) Structural and Electrical Properties of Mechanothermally Synthesized NiFe2O4 Nanoceramics. *Journal of Electronic Materials* 43, 3539 , https://doi.org/10.1007/s11664-014-3216-0
[31] Pattanayak S, Choudhary R.N.P., Das P.R. (2014) Effect of Praseodymium on Electrical Properties of BiFeO3 Multiferroic. *Journal of Electronic Materials* 43, 470-478, https://doi.org/10.1007/s11664-013-2847-x
[32] Garbarz-Glos B, Bąk W, Antonova M, Pawlik M (2013) Structural, microstructural and impedance spectroscopy study of functional ferroelectric ceramic materials based on barium titanate. *Materials Science and Engineering* 49, 012031
[33] Mishra R K, Choudhary R N P, Banerjee A (2010) Bulk permittivity, low frequency relaxation and the magnetic properties of Pb(Fe1/2Nb1/2)O3 ceramics. *J. Phys.: Condens. Matter* 22, 025901 , https://doi.org/10.1088/0953-8984/22/2/025901
[34] Xia J, Zhao Qing, Gao Bo et al. (2014) Sintering temperature and impedance analysis of Mn0.9Co1.2Ni0.27Mg0.15Al0.03Fe0.45O4 NTC ceramic prepared by W/O microemulsion method. *Journal of Alloys and Compounds* 617, 228–234 , https://doi.org/10.1016/j.jallcom.2014.07.149
[35] Purohit V, Padhee R, Choudhary R.N.P. (2018) Dielectric and impedance spectroscopy of Bi(Ca0.5Ti0.5)O3 ceramic *Ceramics International*, 44, 3993-3999 , https://doi.org/10.1016/j.ceramint.2017.11.194
[36] Kumar A., Choudhary R. N. P. (2007) Characterization of electrical behaviour of Si modified BaSnO3 electroceramics using impedance analysis. *J of material SCI: Mater electron*, 42, 2476–2485
[37] Sutar B. C., Das P R., Choudhary R. N. P. (2014) Synthesis and electrical properties of $Sr(Bi_{0.5}V_{0.5})O_3$ electroceramic, *Adv. Mat. Letters* 5, 131-137 , https://doi.org/10.5185/amlett.2013.fdm.51
[38] MacDonald J. R. (1984) Note on the parameterization of the constant-phase admittance element. *Solid State Ionics* 13, 147-149 https://doi.org/10.1016/0167-2738(84)90049-3

Author Bibliography:

Sugato Hajra is working in the field of piezoelectric, lead free piezoelectric materials and energy harvesting techniques. He has published three books with international publishing house: LAP LAMBERT ACADEMIC PUBLICATION in field of Power Plant Engineering, Materials and Instrumentation Engineering.

Sushrisangita Sahoo is pursuing her Ph.D. Degree under the guidance of Prof. P K Mahapatra and Prof. R.N.P. Choudhary in ITER, SOA deemed to be University, Bhubneswar, Odisha, India. She is working in the field of multiferroic materials.

Pravat Rout is working as a Professor in the Department of EEE, ITER, SOA University, Bhubaneswar, Odisha, India. His research interests are soft computing and evolutionary computing techniques and it is application to power system, planning, operation and control.

RNP Choudhary is currently a professor of physics in ITER, SOA University, Bhubneswar, Odisha, India. His broad research interests include structure, microstructure, thermal, ferroelectrics, pyroelectrics, piezoelectrics, thermoelectrics and electrical (impedance) properties of multifunctional/advanced materials (single crystals, ceramics and thin films), ceramics-polymer nanocomposites, liquid crystals, etc. He has received several awards and distinctions from national/international bodies.

